Amyloid Beta-Weighted Cortical Thickness: A New Imaging Biomarker in Alzheimer's Disease

Chan Mi Kim[1,2], Jihye Hwang[1], Jong-Min Lee[3], Jee Hoon Roh[1*], Jae-Hong Lee[1*], Jae-Young Koh, and Alzheimer's Disease Neuroimaging Initiative (ADNI)[#]

[1]*Department of Neurology, Asan Medical Center, University of Ulsan College of Medicine, Seoul, South Korea;* [2]*Department of Medical Engineering, Asan Medical Center, University of Ulsan College of Medicine, Seoul, South Korea;* [3]*Department of Biomedical Engineering, Hanyang University, P.O. Box 55, Sungdong, Seoul, 133-605, South Korea*

Jee Hoon Roh

Jae-Hong Lee

Abstract: Alzheimer's disease (AD) is the most common neurodegenerative disorder pathologically characterized by amyloid-beta (Aβ) plaques and neurofibrillary tangles. The aggregation of Aβ precedes tau pathologies in AD; however, the causal relation between the two pathologies and the mechanisms by which aggregated forms of Aβ contribute to cortical thinning are not fully understood. We proposed quantitative Aβ-weighted cortical thickness analysis to investigate the regional relationship between cortical thinning and amyloid plaque deposition using magnetic resonance (MR) and Pittsburg Compound B (PiB) positron emission tomography (PET) images in patients with AD, mild cognitive impairment (MCI), and subjects with normal cognition. We hypothesized that there are cortical areas that have prominent changes associated with Aβ deposition and there are areas that are relatively independent from Aβ deposition where pathologies other than Aβ (such as tau) are predominant. The study was performed using MRI and PiB PET data from the Alzheimer's Disease Neuroimaging Initiative. We measured accuracy of classification models in three different pairs of groups comparing AD, MCI, and normal cognition. Classification models that used Aβ-weighted cortical thickness were not inferior to classification models that used only cortical thickness or amyloid deposition. In addition, based on timing of changes in cortical thinning and Aβ deposition such as Aβ deposition after cortical thinning; cortical thinning after Aβ deposition, or concurrent Aβ deposition and cortical thinning, we identified three types of relationships between cortical thinning and Aβ deposition: (1) Aβ-associated cortical thinning; (2) Aβ-independent cortical thinning; and (3) Aβ deposition only without cortical thinning. Taken together, these findings suggest that Aβ-weighted cortical thickness values can be used as an objective biomarker of structural changes caused by amyloid pathology in the brain.

Keywords: Alzheimer's disease, Amyloid beta, amyloid imaging, Aβ-weighted cortical thickness, magnetic resonance imaging, mild cognitive impairment, normal cognition, tau.

1. INTRODUCTION

Alzheimer's disease (AD) is the most common neurodegenerative disorder clinically characterized by cognitive worsening and impaired daily activities. Two pathological hallmarks of AD are amyloid-beta (Aβ) plaques, formed by aggregation of Aβ peptides, and neurofibrillary tangles, composed of aggregated forms of tau proteins in the brain [1, 2]. The aggregation of Aβ is known to precede tau pathology in AD, but the relation between the two pathologies remains

Address correspondence to these authors at the Department of Neurology, Asan Medical Center, University of Ulsan College of Medicine, 88 Olympic-ro 43-gil, Songpa-gu, Seoul 138-736, Korea; Tel: +82-2-3010-3443; Fax: +82-2-474-4691; E-mail: roh@amc.seoul.kr; alzheimer@naver.com and Tel: +82-2-3010-3446; Fax: +82-2-474-4691; E-mail: jhlee@amc.seoul.kr

elusive [3, 4]. For example, aggregated forms of tau can be seen in autopsy findings of normal elderly individuals before amyloid plaques emerge [3, 4]. Moreover, the brain regions vulnerable to tau and Aβ pathologies are distinct, although there are overlaps in the advanced stages of AD [5]. Aβ plaques begin and continue to accumulate until they reach a plateau in the association cortices, including the frontal, temporal, parietal, and posterior cingulate cortices, but accumulate only modestly in the medial temporal areas, even in advanced stages of the disease. By contrast, tau-associated pathologies begin in the medial temporal lobe, including the transentorhinal and entorhinal cortices, where they continues to be accumulated with the most significant amount of pathologies by the end of the disease [5].

Many magnetic resonance (MR) imaging studies of patients with AD demonstrated specific volume loss or cortical atrophy patterns with disease progression; however, amyloid pathology based cortical thickness alterations were not investigated thoroughly due to limited access to pathologies at the time of brain MR imaging [6-8]. Recent advances in

amyloid imaging driven by Pittsburgh compound B positron emission tomography (PiB-PET) have enabled *in vivo* imaging of fibrillar forms of Aβ in human brains, and this imaging shows that the distribution of fibrillar forms of Aβ match well with the pathologic accumulation of Aβ plaques [9, 10]. Although Aβ is a primary factor in the pathological progression of AD, the causal relations between Aβ deposition and cortical thinning remain somewhat controversial, with possible contributions of tau and other pathologies. Several studies showed an association between Aβ accumulation and cortical thinning as well as between Aβ accumulation and hippocampal atrophy in patients with AD [11, 12], and in subjects with normal cognition (NC) [12-15]. However, the results are sometimes conflicting such that some studies indicated no association between Aβ and cortical thickness [16, 17].

In this study, we proposed an Aβ-weighted cortical thickness analysis to investigate the regional relationship between cortical thinning and amyloid plaque deposition across whole cortical areas using both MR and PiB-PET images in patients with AD, mild cognitive impairment (MCI), and subjects with NC. We hypothesized that there are cortical areas that have prominent changes associated with Aβ accumulation, such as the association cortices, including prefrontal and posterior cingulate cortices, and there are areas that are relatively independent of Aβ accumulation, such as the medial temporal lobes, where pathologies other than Aβ (such as tau) predominantly accumulate [12]. We categorized the patterns of Aβ-weighted cortical thickness as three types, such as Aβ-associated cortical thinning, Aβ-inde-

pendent cortical thinning, and Aβ deposition without cortical thinning, by the relationships between cortical thinning and Aβ deposition. It was based on three modes of the appearance of pathologies in cortices such that whether the Aβ deposition in specific regions occurred before cortical thinning appeared or occurred after cortical thinning appeared or they occurred at the same time. We measured accuracy of classification models in three different pairs of groups comparing AD, MCI, and NC, to demonstrate that classifications using Aβ-weighted cortical thickness values are not inferior to classifications based on conventional cortical thickness or amyloid imaging analysis.

2. MATERIALS AND METHODS

2.1. Data Acquisition

We investigated a total of 21 AD, 56 MCI, and 18 NC subjects from the Alzheimer's Disease Neuroimaging Initiative (ADNI) database [18] (http://www.loni.ucla.edu/ADNI/) with six AD subjects from Asan Medical Center who completed T1-weighted MRI and PiB-PET dataset. We excluded nine patients with AD and one subject with NC from the ADNI GO dataset because of technical limitations, including co-registration error, failures of cortical surface modeling, and lack of the required size of field of view around neocortex. The demographic characteristics of all subjects are described in Table **1**.

The data sets included high-resolution T1-weighted MR images acquired in the sagittal plane using a magnetization-prepared rapid gradient-echo sequence with 0.94×0.94 mm

Table 1. Demographic information of participants.

	AD		MCI		NC	
Number of subjects	21		56		18	
Gender (M:F)	9:12[*]		33:23[§]		10:8	
Age (year ± s.d.)	70.15 (±9.78)[*]		75.23 (±6.99)[§*]		78.23 (±5.40)	
Education (year ± s.d.)	12.71 (±3.72)[*]		16.49 (±2.82)		16.14 (±2.59)	
ICV (cm³ ± s.d.)	1331357.99 (±158081.19)[*]		1333574.92 (±157915.57)[§]		1334021.90 (±104231.56)	
MMSE (± s.d.)	20.24 (±4.75)[*]		28.61 (±3.27)[§]		28.47 (±1.50)[†]	
CDR (IQR)	1.0 (0.5-1.0)[*]		0.55 (0.5-0.5)[§]		0.00 (0.0-0.0)	
GDS (± s.d.)	2.64 (±1.86)[*]		2.10 (±2.17)		0.84 (±1.21)[†]	
FAQ (± s.d.)	15.09 (±7.67)[*]		5.81 (±5.72)[§]		1.33 (±3.37)[†]	
NPI-Q (± s.d.)	6.25 (±6.84)		3.19 (±3.68)		1.74 (±2.24)	
APOE4 carrier (%)	7 (43.8%)		31 (55.4%)		5 (27.8%)	
PIB positive (%)	21 (100%)		38 (67.9%)		8 (44.4%)	
Global SUVR (± s.d.)	PiB (+)	PiB (-)	PiB (+)	PiB (-)	PiB (+)	PiB (-)
	2.12 (±0.32)	N.A.	2.14 (±0.35)	1.37 (±0.09)	1.63 (±0.07)	1.30 (±0.09)

[*]Statistically significant difference from NC, [§]statistically significant difference from AD, [†]statistically significant difference from MCI.
Abbreviations: AD, Alzheimer's disease; MCI, mild cognitive impairment; NC, normal controls; ICV, intracranial volume; MMSE, mini-mnetal status examination; CDR, clinical dementia rating; GDS, global deterioration scale; FAQ, functional assessment questionnaire total score; NPI-Q, neuropsychiatric inventory-questionnaire total score; s.d., standard deviation; IQR, inter-quartile ratio.

pixel size and 1.2 mm slice thickness. All T1-weighted MR images were acquired using a 1.5-T Philips Medical Systems scanner. PET scans were acquired for 20 minutes, 50–70 min after intravenous injection of 15 ± 1.5mCi 11C-PiB. PET scans were acquired using one of several PET scanners: GE Medical system, Siemens/CTI, or Siemens ECAT. The PET images were reconstructed with 1.22×1.22 mm pixel size and 1.22 mm slice thickness or 2.06×2.06 mm pixel size and 2.43 mm slice thickness depending on scanner types. Detailed information is available from the ADNI website (http://www.loni.ucla.edu/ADNI/).

The datasets for the six patients with AD from Asan Medical Center included high-resolution T1-weighted MR images acquired in the sagittal plane using a three-dimensional T1-weighted turbo field echo sequence with 1.0×1.0 mm pixel size and 1.0 mm slice thickness. All T1-weighted MR images were acquired using a 1.5-T Philips Intera scanner with 2.34×2.34 mm pixel size and 3.27 mm slice thickness. PET scans were 20 min in duration and were acquired starting 60 min after intravenous injection of 16.2 ± 3mCi 11C-PiB. PET scans were acquired using a three-dimensional scanning mode of the Discovery STe PET/computed tomography scanner (GE Medical Systems, Milwaukee, WI, USA) with CT-based attenuation correction. Detailed information is available in our previous report [19].

The Institutional Review Board of Asan Medical Center approved the study protocol, and all the data obtained from the ADNI were analyzed according to the guidelines indicated by the ADNI.

2.2. MR Image Processing

All MR images were processed using the standard Montreal Neurological Institute CIVET pipeline (version1.1.9) (http://wiki.bic.mni.mcgill.ca/index.php/CIVET) to measure cortical thickness. First, the inhomogeneous bias fields from the native MR images were estimated using the N3 algorithm to obtain the distribution of the true intensities [20]. The native MR images were then registered into standardized stereotaxic space using a linear transformation and classified into white matter (WM), gray matter (GM), cerebrospinal fluid (CSF) and background using a neural-net classifier [21]. The surfaces of the inner and outer cortex were automatically fitted using the Constrained Laplacian-Based Automated Segmentation with Proximities (CLASP) algorithm [22]. Finally, hemispheric cortical surfaces consisted of a triangular mesh of 81,920 elements that had the same number of inner and outer vertices were obtained. The Euclidean distance between linked vertices on the inner WM/GM surface and the outer GM/CSF intersection surface was used to measure cortical thickness [23, 24].

2.3. Surface-Based PET Image Processing

All PiB-PET images were processed using FMRIB's Software Library (FSL) and MATLAB (version 7.14; Math Works Inc., Cambridge, MA, USA). The PiB-PET images were resampled to 1mm³ isovoxels to estimate the resolution problems derived from multiple scanner types. Each individual PiB-PET image was co-registered into the corresponding native MR image using rigid-body registration with a mutual information cost function within FMRIB's Software Library.

Cerebellum GM in the MR image was segmented using atlas-based non-linear registration, and the PiB-PET image was scaled using the mean value in the cerebellum GM to create the standardized uptake value ratio (SUVR) image [25, 26]. The PiB value in each vertex of the cortical surface was calculated using the mean of the interpolated values along the column line between the outer GM/CSF and inner GM/WM vertices. The mean PiB value of each column line was obtained by subvoxel resampling at five proportions using a trilinear interpolation performed in MATLAB (version 7.14; Math Works Inc., Cambridge, MA, USA). The GM partial volume estimation map (mPVE) was obtained from the MR image for the portion of GM within each voxel due to the fact that PiB mainly accumulates in GM [27, 28]. Each mPVE was smoothed with a Gaussian kernel of 8 mm full-width half-maximum (FWHM) to adapt point spread functions in PET, and the mean mPVE value of each column line was obtained by subvoxel resampling at five proportions using a trilinear interpolation [29, 30]. Each PiB-SUVR value in each vertex was then divided by the corresponding mPVE value. Consequently, we obtained a partial-volume-corrected PiB-SUVR value in each vertex on the cortical surface. For statistical analysis, each PiB-SUVR surface map was registered to a surface template using sphere-to-sphere warping surface registration after diffusion smoothing with 20 mm FWHM for statistical analysis [31, 32].

2.4. Calculation of Aβ-Weighted Cortical Thickness

In each vertex, we calculated normalized z-scores of cortical thickness and Aβ deposition to use each variable irrespective of multimodal variables obtained from MR and PET scanners [33]. The normalized z-score of the *i-th* vertex of each subject *k* was defined as follows:

$$Z_k^{thickness}(i) = \frac{X_k^{thickness}(i) - \mu_{normal}^{thickness}(i)}{\sigma_{normal}^{thickness}(i)} \tag{1}$$

$$Z_k^{A\beta}(i) = \frac{X_k^{A\beta}(i) - \mu_{normal}^{A\beta}(i)}{\sigma_{normal}^{A\beta}(i)} \tag{2}$$

where the $X_k(i)$ denotes the *i-th* vertex of each subject *k*. The mean and standard deviations of healthy subjects were $\mu_{normal}(i)$ and $\sigma_{normal}(i)$. According to these equations, normalized z-scores of cortical thickness and Aβ deposition have three types of values: such as positive, negative and zero. Before calculating the Aβ-weighted cortical thickness values, we converted all normalized z-scores of Aβ deposition into positive values. To do this, we calculated the minimum value of the normalized z-score of Aβ deposition in all subjects, and then converted the normalized z-scores of Aβ deposition into positive values in decimal using three types of equations (Eq. 3). The Aβ-weigh value of the *i-th* vertex of each subject *k* is given as follows:

$$w_k^{A\beta}(i) = \begin{cases} 1 - \left(\frac{1}{\left[\left| Z^{A\beta\min} \right| \right]} \times \left| Z_k^{A\beta}(i) \right| \right), & Z_k^{A\beta}(i) < 0 \\ \\ 1, & Z_k^{A\beta}(i) = 0 \\ \\ 1 + \left(\frac{1}{\left[\left| Z^{A\beta\min} \right| \right]} \times \left| Z_k^{A\beta}(i) \right| \right), & Z_k^{A\beta}(i) > 0 \end{cases} \tag{3}$$

where $Z^{A\beta min}$ is minimum value of the normalized z-score of Aβ over all subjects. Therefore, Aβ-weighted values, W(*i*), between zero to one indicate that Aβ deposition is less than the average amount of Aβ deposition of the NC group. An Aβ-weighted value of zero indicates that the amount of Aβ deposition is equal to the amount in the NC group, and an Aβ-weighted value greater than 1 indicates more Aβ deposition than the mean Aβ deposition of the NC group. The Aβ-weighted cortical thickness value of the *i-th* vertex of each subject *k* was then calculated as follows:

$$Y_k^{A\beta-weighted\ Cth}(i) = Z_k^{thickness}(i) \times W_k^{A\beta}(i) \qquad (4)$$

2.5. Classification Using Linear Discriminant Analysis

We constructed multivariate classifier models using Aβ-weighted cortical thickness and measured the classification accuracy of these models to determine whether Aβ-weighted cortical thickness was non-inferior to analysis using cortical thickness only or Aβ uptakes only as a new biomarker for AD. We used Fisher's linear discriminate analysis (LDA) to create the classifier between three pairs of groups, which performed an adjustment to maximize the between-class variance and minimizes the within-class variance until it finds the axes that maximally separate the groups [34]. We defined the features as Aβ-weighted cortical thickness values within pre-defined 52 regions-of-interest (ROI), which were widely known as the cortical signature of AD [11] to reduce the feature dimensions in each classifier (Supplementary Table **2**). These cortical signatures were segmented within the cortical surface by an automated anatomical labeling (AAL) template [35]. The volume-based AAL template originally defined on a single subject was registered into the standard surface model by two-dimensional surface registration [36], then the 78 AAL labels were aligned to the cortical surface of each individual using sphere-to-sphere warping registration. Leave-one-out cross-validation was performed to evaluate the constructed classifiers by measuring the classification accuracy from the three pairs: AD-NC, AD-MCI, and MCI-NC. It assigned one subject as the testing set and

used the remaining subjects as the training sets for the LDA classifier [37]. The cross-validation process was repeated 5,000 times to avoid selection bias in each classifier.

2.6. Statistical Analysis

Cortical thicknesses and Aβ-weighted cortical thickness values across whole cortical vertices were compared across the three groups after controlling for age, sex, education level, and intra-cranial volume (ICV) using a general multivariate linear model within Surf Stat packages. To solve the multiple comparisons problem, we performed false discovery rate (FDR) correction at a q value of 0.05 [38]. We also calculated mean cortical thickness, mean Aβ-weighted cortical thickness, and mean PiB deposition in each of the 78 cortical regions derived from the AAL template and compared these between the three groups using two sample t-tests after controlling for age, sex, education level, and ICV [39]. In ROI-based analysis, we applied Bonferroni correction to correct for multiple comparisons [40].

3. RESULTS

3.1. Clinical Characteristics of Subjects

The mean age of MCI subjects is older than AD patients (75.23 (± 6.99) in MCI versus 70.15 (±9.78) in AD, p < 0.001). There were significant gender difference between patients with AD and NC subjects. Patients with MCI and AD demonstrated worse performance of neuropsychological tests, less education levels, and lower intracranial volume compared to NC subjects. In neuropsychological tests, the mini-mental state examination (MMSE), clinical dementia rating (CDR), global deterioration scale (GDS), and functional assessment questionnaire total score (FAQ) revealed statistical difference across NC, MCI, and AD groups. There were no significant neuropsychiatric inventory-questionnaire total score (NPI-Q) group difference between three groups. Detailed demographic characteristics of all subject groups and the results of neuropsychological tests are described in Table **1**.

Table 2.   Classification datasets results.

Features		AD vs NC	AD vs MCI	MCI vs NC
Cortical Thickness	**Accuracy**	84.2%	86.5%	75.2%
	Sensitivity	89.2%	78.6%	81.8%
	Specificity	79.2%	88.6%	51.3%
Amyloid PET	**Accuracy**	90.6%	81.9%	74.6%
	Sensitivity	89.5%	76.6%	76.9%
	Specificity	91.6%	83.5%	66.3%
Amyloid beta-weighted cortical thickness	**Accuracy**	86.3%	87.6%	76.2%
	Sensitivity	86.0%	76.5%	81.7%
	Specificity	86.6%	90.7%	56.6%

Abbreviations: AD, Alzheimer's disease; MCI, mild cognitive impairment; NC, normal controls; vs, versus.
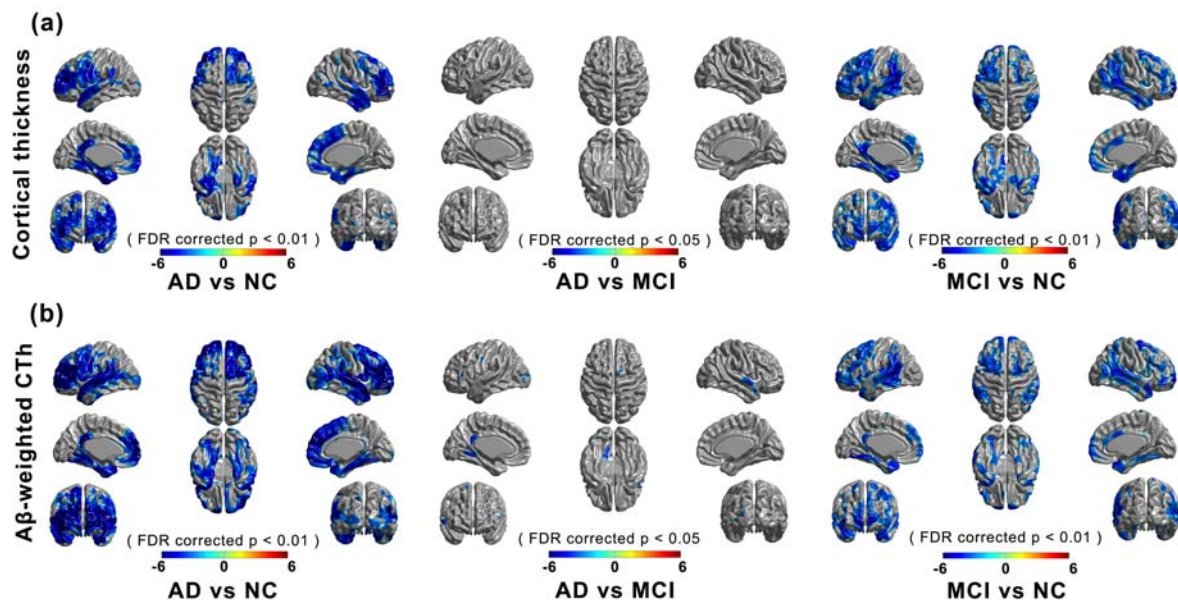
Fig. (1). *De novo* cortical thickness (CTh) patterns (**a**) and Amyloid beta (Aβ)-weighted cortical thickness patterns (**b**) in subjects with AD, MCI, and NC across whole cortical vertices. Abbreviations: AD, Alzheimer's disease; MCI, mild cognitive impairment; NC, normal cognition.

3.2. *De novo* Cortical Thickness, A β-Weighted Cortical Thickness, and PiB Deposition Patterns

We obtained statistically significant group differences in cortical thickness as well as Aβ-weighted cortical thickness patterns among three groups while controlling for age, gender, and ICV (Fig. **1**). Compared to NC subjects, patients with AD had more cortical thinning in both superior temporal gyri, parts of the right middle and inferior temporal gyri, both frontal cortices, part of the left supramarginal gyrus, both temporal poles, the left posterior cingulate cortex, and part of the lateral occipital gyri (Fig. **1a**, left column). Patients with MCI had more cortical thinning in both superior parietal cortices, parts of the middle frontal cortex, both middle temporal gyri, both temporal poles, the left posterior cingulate, parts of both supramarginal gyri, and both inferior parietal gyri (Fig. **1a**, middle column). There were no significant differences in cortical thickness between patients with AD and patients with MCI (Fig. **1a**, right column).

Aβ-weighted cortical thickness analyses indicated more cortical thinning in patients with AD and patients with MCI than in subjects with NC (Fig. **1b**). In AD patients, the pattern of Aβ-weighted cortical thickness was similar to the pattern of *de novo* cortical thinning but with more significant thinning in both superior temporal gyri, both middle frontal gyri, the right superior frontal gyrus, both lateral occipital-gyri, and the right fusi form gyrus (q < 0.05, FDR corrected; Fig. **1b**, left column). There was almost the same pattern of group differences between patients with MCI and subjects with NC (q < 0.05, FDR corrected; Fig. **1b**, right column). Patients with AD had additional atrophy in the left postcentral gyri, part of the left lingual gyrus, and part of the right superior temporal gyri compared to patients with MCI (q < 0.05, FDR corrected; Fig. **1b**, middle column).

The amount of Aβ accumulation was measured in each vertex of cortical areas using the SUVR (Fig. **2**). Compared to subjects with NC, patients with AD had statistically greater PiB deposition in almost all cortical regions except for parts of the left central gyrus, both temporal poles, both para hippocampal gyri, both entorhinal cortices, and parts of both lateral occipital lobes (q < 0.01, FDR corrected; Fig. **2a**). Similar patterns of PiB deposition were present in patients with MCI, with greater PiB deposition than subjects with NC in almost all cortical regions except parts of both superior frontal gyri (q < 0.01, FDR corrected; Fig. **2c**). Similar to the cortical thickness analyses, there were few regions where PiB deposition was significantly different between patients with AD and patients with MCI (q < 0.01, FDR corrected; Fig. **2b**).

3.3. ROI-Based Cortical Thickness, Aβ-Weighted Cortical Thickness, and PiB Deposition

To further investigate the clinical implication of Aβ-weighted cortical thickness, we grouped cortical regions based on the relationships of *de novo* cortical thinning, *de novo* PiB retention, and Aβ-weighted cortical thickness. Using the AAL template, five distinct patterns of Aβ-related cortical thickness were defined in Fig. (**3**). First, we grouped cortical patterns into three types of relationships: (1) Aβ-independent cortical thinning (Fig. **3a**); (2) Aβ-associated cortical thinning (Fig. **3b–d**); and (3) Aβ deposition only (Fig. **3e**). Then, we further divided Aβ-associated cortical thinning into three distinct patterns based on the timing of the Aβ-associated cortical thinning: the first where the cortical thinning may begin with other causes and then accelerate with accumulation of Aβ in the brain (Fig. **3b**); the second where the Aβ-associated cortical thinning occurs even in MCI (Fig. **3c**); and the third where Aβ-associated cortical
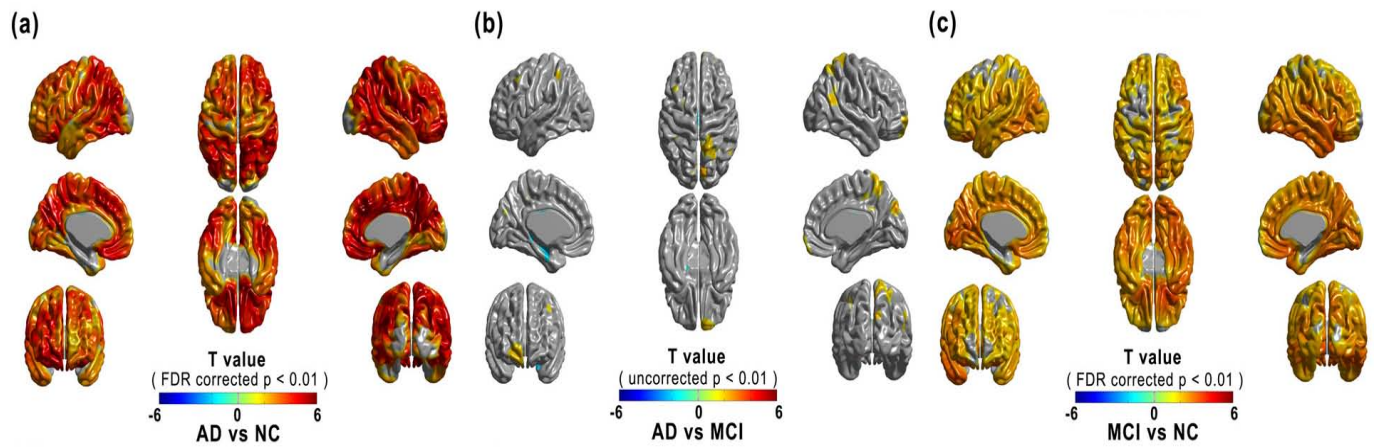
Fig. (2). Comparison of amyloid-beta (Aβ) uptake patterns among subjects with AD, MCI, and NC. Abbreviations: AD, Alzheimer's disease; MCI, mild cognitive impairment; NC, normal cognition.
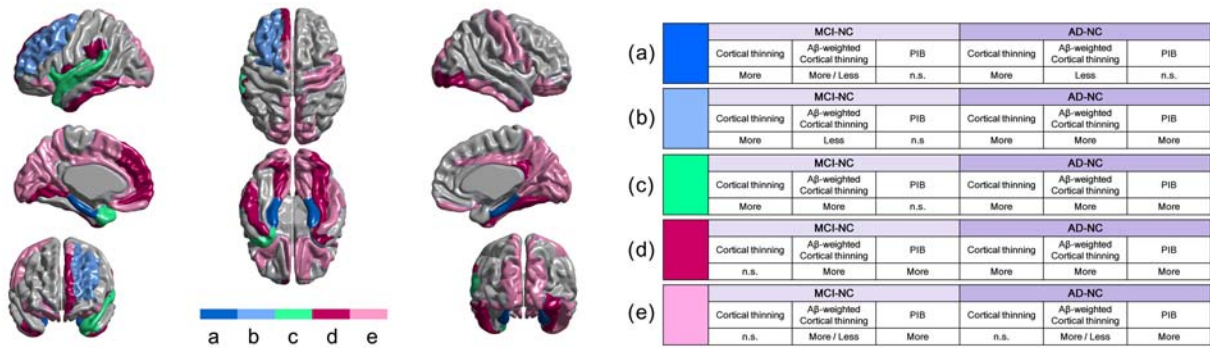

	MCI-NC			AD-NC		
(a)	Cortical thinning	Aβ-weighted Cortical thinning	PIB	Cortical thinning	Aβ-weighted Cortical thinning	PIB
	More	More / Less	n.s.	More	Less	n.s.
(b)	Cortical thinning	Aβ-weighted Cortical thinning	PIB	Cortical thinning	Aβ-weighted Cortical thinning	PIB
	More	Less	n.s	More	More	More
(c)	Cortical thinning	Aβ-weighted Cortical thinning	PIB	Cortical thinning	Aβ-weighted Cortical thinning	PIB
	More	More	n.s.	More	More	More
(d)	Cortical thinning	Aβ-weighted Cortical thinning	PIB	Cortical thinning	Aβ-weighted Cortical thinning	PIB
	n.s.	More	More	More	More	More
(e)	Cortical thinning	Aβ-weighted Cortical thinning	PIB	Cortical thinning	Aβ-weighted Cortical thinning	PIB
	n.s.	More / Less	More	n.s.	More / Less	More

Fig. (3). Five patterns of amyloid beta (Aβ)-weighted cortical thickness patterns based on comparison of amyloid uptake and cortical thinning in the three groups of subjects. (**a**) Aβ-independent cortical thinning; (**b**) Aβ-associated cortical thinning: non-Aβ associated thinning in MCI followed by Aβ-associated thinning in AD; (**c**) Aβ-associated cortical thinning: A βassociated thinning in MCI followed by more A β-associated thinning in AD; (**d**) Aβ-associated cortical thinning: early Aβ-driven thinning in MCI followed by continuous Aβ-driven thinning in AD; (**e**) Aβ deposition only. Abbreviations: AD, Alzheimer's disease; MCI, mild cognitive impairment.

thinning is Aβ-driven (Fig. **3d**). In this third subgroup, no *de novo* cortical thinning was noted compared to subjects with NC, but Aβ-weighted cortical thinning was noted at MCI stage (Fig. **3d**). Details of Aβ-weighted cortical thickness, *de novo* cortical thinning, and amyloid deposition measured by PiB-PET are provided in Fig. (**3**) and Supplementary Table **1**.

(a) Aβ-Independent Cortical Thinning

These regions demonstrated no difference in PiB uptake between subjects with NC, patients with MCI, and NC and even between AD and NC. *De novo* cortical thinning was more prominent than Aβ-weighted cortical thinning in all comparisons. Regions with Aβ-independent cortical thinning included the left and right parahippocampal gyri.

(b) Aβ-Associated Cortical Thinning: Non-Aβ Associated Thinning in MCI Followed by Aβ-Associated Thinning in AD

In these regions, no difference in PiB uptake was noted between patients with MCI and subjects with NC. *De novo* cortical thinning was more prominent than Aβ-weighted cortical thinning in patients with MCI. With PiB uptake in AD,

Aβ-weighted cortical thinning became more prominent as well as *de novo* cortical thinning. Regions in this category included the left middle frontal gyrus, right superior frontal gyrus, and bilateral parahippocampal gyri.

(c) Aβ-Associated Cortical Thinning: Aβ-Associated Thinning in MCI Followed by More Aβ-Associated Thinning in AD

These regions demonstrated no difference in PiB uptake between patients with MCI and subjects with NC. More Aβ-weighted cortical thinning than d*e novo* cortical thinning was noted in patients with MCI. With PiB uptake in AD, Aβ-weighted cortical thinning as well as *de novo* cortical thinning became more prominent. Regions in this category included the left insula, left superior, and middle temporal gyri, and left temporal pole.

(d) Aβ-Associated Cortical Thinning: Early Aβ-Driven Thinning in MCI Followed by Continuous Aβ-Driven Thinning in AD

These regions demonstrated more PiB uptake in patients with MCI compared to NC. More Aβ-weighted cortical thinning over *de novo* cortical thinning was noted in patients

with MCI. With more PiB uptake in AD, Aβ-weighted cortical thinning as well as *de novo* cortical thinning became more prominent. Regions in this category included the left superior frontal gyrus (medial part), right posterior cingulate gyrus, left lingual gyrus, right inferioroccipital gyrus, right fusiform gyrus, left supramarginal gyrus, right temporal pole, and left inferior temporal gyrus.

(e) Aβ Deposition Only

More PiB uptake in patients with MCI and patients with AD compared to NC was noted in the fifth group. No prominent Aβ-weighted cortical thinning as well as *de novo* cortical thinning was noted in patients with AD and MCI. Regions in this category have relative independence to Aβ-associated pathology and included the primary cortices (right precentral gyrus, right postcentral gyrus, bilateral calcarine fissure and surrounding cortices, bilateral cuneus, and bilateral olfactory cortex) and the right superior frontal gyrus, bilateral inferior frontal gyri (orbital and opercular parts), left supplementary motor area, bilateral gyrus rectus, left anterior and bilateral median cingulate and paracingulate gyri, right lingual gyrus, bilateral occipital gyrus, right inferior temporal gyrus, and bilateral precuneus.

3.4. Classification Analysis

We used linear discriminant analysis to test the classification accuracy of multivariate classifiers that used cortical thickness, Aβ deposition, and Aβ-weighted cortical thickness within 52 cortical areas. The accuracy, sensitivity, and specificity of Aβ-weighted cortical thickness were not inferior to conventional classification using only cortical thickness or Aβ uptake (Table **2**).

4. DISCUSSION

In this study, we incorporated information on the amount of Aβ into a measurement of cortical thickness by developing an Aβ-weighted measure of cortical thickness. We classified patterns of Aβ-weighted cortical thickness by comparing *de novo* cortical thinning, *de novo* Aβ uptake and Aβ-weighted cortical thickness between subjects with AD, MCI, and NC. The brain regions in which cortical thinning was aggravated or expanded by Aβ-weighting matched well with the brain areas where Aβ first accumulates and then progresses in the brain. Finally, the classification model that used Aβ-weighted cortical thickness was not inferior to the models that used cortical thickness or amyloid uptake alone.

There were more significant group differences in some cortical regions when weighting Aβ pathology, such as the left posterior cingulate cortex and both inferior parietal gyri. These results are consistent with previous reports that the inferior parietal lobule and posterior cingulate cortex have a strong relation with cortical thinning and Aβ deposition. These brain regions are also known as cortical hub regions of the brain's default network and are associated with memory-related functions in clinically normal elderly individuals [12]. In addition, we observed diverse associations between *de novo* cortical thinning, *de novo* amyloid uptake, and Aβ-weighted cortical thickness. Some regions appeared to have more cortical thinning with lower p values in analyses performed with Aβ-weighted cortical thickness than in analyses performed with *de novo* cortical thickness. On the other hand, other regions had higher p values in analyses performed with Aβ-weighted cortical thickness than in analyses performed with *de novo* cortical thickness. Given that these changes were noted in patients with MCI, patients with AD, or both, we conclude that, in different stages of the disease, some cortical regions were affected by Aβ accumulation, whereas others were not affected. Based on these findings, we identified five distinctive patterns of Aβ-weighted cortical thickness. First, we found that both parahippocampal gyri had significant cortical thinning but lower Aβ levels in patients with MCI and AD (Fig. **3a**). Even in patients with AD, the amount of Aβ-weighted cortical thickness and *de novo* cortical thinning was not different in degree, which suggests a lack of association between cortical thinning and Aβ accumulation in these regions. This suggests that the cortical thinning in these regions may have been driven by pathologies other than Aβ aggregation, such as tau. Second, we found that some cortical regions, such as the left superior frontal gyrus, and dorso lateral and left middle frontal gyrus, had significant cortical thinning without any increase in Aβ uptake in patients with MCI (Fig. **3b**). These regions demonstrated less group difference of Aβ-weighted cortical thickness and *de novo* cortical thickness. These regions had more cortical thinning and Aβ deposition in AD with more prominent changes in Aβ-weighted cortical thickness analysis. This demonstrates that the cortical thinning in these regions occurred before, or independently of, Aβ aggregation but might be accelerated by Aβ deposition in later stages. Third, we found that some regions, such as the left insula, left superior temporal gyrus, and bilateral temporal poles, demonstrated cortical thinning and a similar degree of Aβ-weighted cortical thinning without Aβ deposition in patients with MCI (Fig. **3c**). Given that those regions represented Aβ uptake in AD and kept to represent cortical thinning in AD, soluble forms of Aβ may have affected the cortical thickness in patients with MCI, which might be accelerated with aggregated forms of Aβ in AD. The fourth pattern represented Aβ deposition without cortical thinning in MCI and an increase in cortical thinning as well as Aβ deposition in AD (Fig. **3d**). Regions with this pattern had more Aβ-weighted cortical thinning than *de novo* cortical thinning, which indicates that the Aβ aggregation in these regions occurred before the cortical thinning and it might drive the cortical thinning. Finally, brain regions including the primary cortices had more Aβ deposition but no significant cortical thinning patterns in patients with MCI and AD (Fig. **3e**), suggesting that the cortical thinning in these regions might be independent of Aβ aggregation in the brain.

This quantitative weighting of pathological findings using data from MR images has not been performed previously in subjects with AD spectrum disorders. Given that the Aβ-weighted cortical thickness analysis matched well with pathologic findings and with future changes in cortical thickness in advanced AD, it may improve our understanding of MR and amyloid PET imaging findings. Pathology-weighted cortical thinning may also be useful in other neurodegenerative dementia research to estimate the pathology-associated changes in the brain. The changes in cortical thickness enhanced by weighting of the specific pathologic burden may lead to identification of symptoms that are not

present at the time of imaging, but can be observed in later stage of the disease.

The following limitations of this study should be noted. First, there were no pathological data to confirm our findings. Second, there was a limited number of subjects with both PiB-PET imaging data and MR imaging data in the ADNI dataset that we used. At present, most patients are assessed with 3.0-T MR imaging and AV-45 PET scans; therefore, we were not able to assess additional subjects with both PiB-PET and MR imaging data. A follow-up study with the ADNI2 dataset will enable replication and further investigation of the current findings with increased number of subjects and additional biomarker data. Third, the current study was performed using a cross-sectional dataset; thus we cannot understand the causal relation between the Aβ accumulation and cortical thinning. Fourth, we were not able to assess additional pathologies of AD, such as tau and neuroinflammation. Future studies with additional biomarkers, autopsy findings, or new imaging tracers will allow further understanding of our findings. Fifth, in this study, the mean age of MCI subjects are older than AD patients and the percentage of APOE4 carrier is higher in MCI subjects (55.4%) than in AD subjects. We think this may have attenuated the difference in cortical thickness and in Aβ deposition between AD and MCI. Finally, the classification model that used Aβ-weighted cortical thickness was not inferior, but also not superior, to models that used cortical thickness alone or Aβ uptake alone. We interpreted this as due to the fact that accumulation of Aβ measured by PiB-PET in most brain regions was greater in patients with MCI than in subjects with NC. Therefore, even if there were brain regions that were mainly affected by Aβ-weighted cortical thinning, the classification power of the method was not as significant as the power of Aβ deposition itself which affects most brain regions in MCI status. Future studies with a greater number of subjects would allow more accurate interpretation of the clinical implication of Aβ-weighted cortical thickness.

In conclusion, these findings suggest that the five distinctive regional patterns obtained by Aβ-weighted cortical thickness analysis can objectively indicate brain regions where Aβ accumulation occurs and brain regions where Aβ accumulation affects cortical thickness. Taken together, these findings indicate that Aβ-weighted cortical thickness, which incorporates data from both MR and amyloid PET imaging, is a consistent and objective imaging biomarker in AD.

ABBREVIATIONS

Aβ   =   Amyloid beta

AAL   =   Automated anatomical labeling

AD   =   Alzheimer's disease

ADNI =   Alzheimer's Disease Neuroimaging Initiative

FDR   =   False discovery rate

GM   =   Gray matter

ICV   =   Intra-cranial volume

MCI   =   Mild cognitive impairment

mPVE =   Partial volume estimation map

MR   =   Magnetic resonance

NC   =   Normal cognition

PET   =   Positron emission tomography

PiB   =   Pittsburgh compound B

ROI   =   Regions-of-interest

SUVR =   Standardized uptake value ratio

CONFLICT OF INTEREST

The authors confirm that this article content has no conflict of interest.

ACKNOWLEDGEMENTS

SUPPLEMENTARY MATERIALS

Supplementary material is available on the publishers web site along with the published article.

REFERENCES

[1]   Tiraboschi P, Hansen LA, Thal LJ, Corey-Bloom J. The importance of neuritic plaques and tangles to the development and evolution of AD. Neurology 62(11): 1984-9 (2004).

[2]   Jack CR, Jr., Knopman DS, Jagust WJ, Petersen RC, Weiner MW, Aisen PS, *et al.* Tracking pathophysiological processes in Alzheimer's disease: an updated hypothetical model of dynamic biomarkers. Lancet Neurol 12(2): 207-16 (2013).

[3]　Price JL, Morris JC. Tangles and plaques in nondemented aging and "preclinical" Alzheimer's disease. Ann Neurol 45(3): 358-68 (1999).

[4]　Price JL, Morris JC. So what if tangles precede plaques? Neurobiol Aging 25(6): 721-3; discussion 43-6 (2004).

[5]　Braak H, Braak E. Neuropathological stageing of Alzheimer-related changes. Acta Neuropathol 82(4): 239-59 (1991).

[6]　Lerch JP, Pruessner JC, Zijdenbos A, Hampel H, Teipel SJ, Evans AC. Focal decline of cortical thickness in Alzheimer's disease identified by computational neuroanatomy. Cereb Cortex 15(7): 995-1001 (2005).

[7]　Frisoni GB, Fox NC, Jack CR, Jr., Scheltens P, Thompson PM. The clinical use of structural MRI in Alzheimer disease. Nat Rev Neurol 6(2): 67-77 (2010).

[8]　Hampel H, Frank R, Broich K, Teipel SJ, Katz RG, Hardy J, *et al.* Biomarkers for Alzheimer's disease: academic, industry and regulatory perspectives. Nat Rev Drug Discov 9(7): 560-74 (2010).

[9]　Klunk WE, Engler H, Nordberg A, Wang Y, Blomqvist G, Holt DP, *et al.* Imaging brain amyloid in Alzheimer's disease with Pittsburgh Compound-B. Ann Neurol 55(3): 306-19 (2004).

[10]　Kemppainen NM, Aalto S, Wilson IA, Nagren K, Helin S, Bruck A, *et al.* Voxel-based analysis of PET amyloid ligand [11C]PIB uptake in Alzheimer disease. Neurology 67(9): 1575-80 (2006).

[11]　Dickerson BC, Bakkour A, Salat DH, Feczko E, Pacheco J, Greve DN, *et al.* The cortical signature of Alzheimer's disease: regionally specific cortical thinning relates to symptom severity in very mild to mild AD dementia and is detectable in asymptomatic amyloid-positive individuals. Cereb Cortex 19(3): 497-510 (2009).

[12]　Becker JA, Hedden T, Carmasin J, Maye J, Rentz DM, Putcha D, *et al.* Amyloid-beta associated cortical thinning in clinically normal elderly. Ann Neurol 69(6): 1032-42 (2011).

[13]　Fagan AM, Head D, Shah AR, Marcus D, Mintun M, Morris JC, *et al.* Decreased cerebrospinal fluid Abeta(42) correlates with brain atrophy in cognitively normal elderly. Ann Neurol 65(2): 176-83 (2009).

[14]　Storandt M, Mintun MA, Head D, Morris JC. Cognitive decline and brain volume loss as signatures of cerebral amyloid-beta peptide deposition identified with Pittsburgh compound B: cognitive decline associated with Abeta deposition. Arch Neurol 66(12): 1476-81 (2009).

[15]　Fjell AM, Walhovd KB, Fennema-Notestine C, McEvoy LK, Hagler DJ, Holland D, *et al.* Brain atrophy in healthy aging is related to CSF levels of Abeta1-42. Cereb Cortex 20(9): 2069-79 (2010).

[16]　Josephs KA, Whitwell JL, Ahmed Z, Shiung MM, Weigand SD, Knopman DS, *et al.* Beta-amyloid burden is not associated with rates of brain atrophy. Ann Neurol 63(2): 204-12 (2008).

[17]　Chetelat G, Villemagne VL, Pike KE, Baron JC, Bourgeat P, Jones G, *et al.* Larger temporal volume in elderly with high versus low beta-amyloid deposition. Brain : J Neurol 133(11): 3349-58 (2010).

[18]　Carrillo MC, Bain LJ, Frisoni GB, Weiner MW. Worldwide Alzheimer's disease neuroimaging initiative. Alzheimer's Dementia 8(4): 337-42 (2012).

[19]　Lee JH, Kim SH, Kim GH, Seo SW, Park HK, Oh SJ, *et al.* Identification of pure subcortical vascular dementia using 11C-Pittsburgh compound B. Neurology 77(1): 18-25 (2011).

[20]　Sled JG, Zijdenbos AP, Evans AC. A nonparametric method for automatic correction of intensity nonuniformity in MRI data. IEEE Trans Med Imaging 17(1): 87-97 (1998).

[21]　Zijdenbos AP, Forghani R, Evans AC. Automatic "pipeline" analysis of 3-D MRI data for clinical trials: application to multiple sclerosis. IEEE Trans Med Imaging 21(10): 1280-91 (2002).

[22]　Kim JS, Singh V, Lee JK, Lerch J, Ad-Dab'bagh Y, MacDonald D, *et al.* Automated 3-D extraction and evaluation of the inner and outer cortical surfaces using a Laplacian map and partial volume effect classification. NeuroImage 27(1): 210-21 (2005).

[23]　Kabani N, Le Goualher G, MacDonald D, Evans AC. Measurement of cortical thickness using an automated 3-D algorithm: a validation study. NeuroImage 13(2): 375-80 (2001).

[24]　MacDonald D, Kabani N, Avis D, Evans AC. Automated 3-D extraction of inner and outer surfaces of cerebral cortex from MRI. NeuroImage 12(3): 340-56 (2000).

[25]　Sperling RA, Laviolette PS, O'Keefe K, O'Brien J, Rentz DM, Pihlajamaki M, *et al.* Amyloid deposition is associated with impaired default network function in older persons without dementia. Neuron 63(2): 178-88 (2009).

[26]　Johnson KA, Gregas M, Becker JA, Kinnecom C, Salat DH, Moran EK, *et al.* Imaging of amyloid burden and distribution in cerebral amyloid angiopathy. Ann Neurol 62(3): 229-34 (2007).

[27]　Jack CR, Jr., Lowe VJ, Senjem ML, Weigand SD, Kemp BJ, Shiung MM, *et al.* 11C PiB and structural MRI provide complementary information in imaging of Alzheimer's disease and amnestic mild cognitive impairment. Brain : J Neurol 131(Pt 3): 665-80 (2008).

[28]　Price JC, Klunk WE, Lopresti BJ, Lu X, Hoge JA, Ziolko SK, *et al.* Kinetic modeling of amyloid binding in humans using PET imaging and Pittsburgh Compound-B. J Cereb Blood Flow Metab 25(11): 1528-47 (2005).

[29]　Tohka J, Zijdenbos A, Evans A. Fast and robust parameter estimation for statistical partial volume models in brain MRI. NeuroImage 23(1): 84-97 (2004).

[30]　Park HJ, Lee JD, Chun JW, Seok JH, Yun M, Oh MK, *et al.* Cortical surface-based analysis of 18F-FDG PET: measured metabolic abnormalities in schizophrenia are affected by cortical structural abnormalities. NeuroImage 31(4): 1434-44 (2006).

[31]　Lerch JP, Evans AC. Cortical thickness analysis examined through power analysis and a population simulation. NeuroImage 24(1): 163-73 (2005).

[32]　Im K, Lee JM, Lee J, Shin YW, Kim IY, Kwon JS, *et al.* Gender difference analysis of cortical thickness in healthy young adults with surface-based methods. NeuroImage 31(1): 31-8 (2006).

[33]　Raj A, Mueller SG, Young K, Laxer KD, Weiner M. Network-level analysis of cortical thickness of the epileptic brain. NeuroImage 52(4): 1302-13 (2010).

[34]　McLachlan GJ. Discriminant analysis and statistical pattern recognition. Hoboken, N.J. Wiley (2004).

[35]　Tzourio-Mazoyer N, Landeau B, Papathanassiou D, Crivello F, Etard O, Delcroix N, *et al.* Automated anatomical labeling of activations in SPM using a macroscopic anatomical parcellation of the MNI MRI single-subject brain. NeuroImage 15(1): 273-89 (2002).

[36]　Lyttelton O, Boucher M, Robbins S, Evans A. An unbiased iterative group registration template for cortical surface analysis. NeuroImage 34(4): 1535-44 (2007).

[37]　Kohavi R Ed, A study of cross-validation and bootstrap for accuracy estimation and model selection. IJCAI (1995).

[38]　Genovese CR, Lazar NA, Nichols T. Thresholding of statistical maps in functional neuroimaging using the false discovery rate. NeuroImage 15(4): 870-8 (2002).

[39]　Welch BL. The generalisation of student's problems when several different population variances are involved. Biometrika 34(1-2): 28-35 (1947).

[40]　Bonferroni CE. Teoria statistica delle classi e calcolo delle probabilita. USA: Libreria Internazionale Seeber pp. 3-62 (1936).